Comparison of Modelled to Measured High-Resolution ISAR Data

Bert van den Broek[1], Tanja Bieker[2], Lucas van Ewijk[1],

[1]TNO Defense, Security and Safety, Waalsdorperweg 63, 2509 JG The Hague, The Netherlands.
[2]FGAN-FHR, Neuenahrer Straße 20, D-53343 Werthhoven, Germany.

Abstract

We have obtained modelled ISAR data for a ZSU-23-4 air defence unit using a high-fidelity 600,000 facet model and the RAPPORT RCS prediction code. These ISAR data are compared with results from the FERMAT RCS prediction code using the same facet model of the ZSU23-4. In order to analyse how well the prediction results can represent measured ISAR data the modelled data are compared with measured ARL ISAR data of a ZSU-23-4 where the same parameters and resolution have been used. In addition we compare the modelled data with measured ISAR data from other targets than the ZSU-23-4 in order to check whether the measured and modelled data of the same target are more similar compared to data from other targets. We found that modelled and measured data certainly have common characteristics but that they are not similar enough to replace measured by modelled data for the purpose of target discrimination.

1. Introduction

High-resolution ISAR measurements are used to obtain an accurate description of the radar signatures of targets. Such data can also be used as reference data to recognise targets in SAR scenes. Since ISAR measurements are costly and time consuming modelling of ISAR data can be an alternative way to acquire such data. Modelling also allows flexible adaptation of observation parameters such as for example depression angle and resolution.
Of course main question is whether such modelled data resemble the actual measurements sufficiently well. Modelled data and measurements should not only look similar but modelled data should also be suitable for purposes such as target recognition.
Recent years several accurate codes for calculating radar signatures, such as Xpatch, RAPPORT and FERMAT have been developed. Modelled data do not only depend on the details of the algorithm used in the code but also on the details of geometrical description of the target. High fidelity geometrical descriptions of objects are available now and in addition computing time has become acceptable due to the constantly increasing computer power. Because of this we have been able to compute with the RAPPORT code high-resolution ISAR data using a 600,000 high fidelity facet model for the geometrical description. Parameters for the ISAR data were chosen to exactly match ISAR measurements of the ZSU23-4 performed by ARL. Also, similar data has been generated by Onera using the FERMAT code and using the same facet model.
In this study we compare the modelled data and the measurements to determine whether modelled can be used for target recognition. For that purpose similar features from both modelled data and measurements are extracted and used in a target discrimination procedure. In this paper we first give a description of the RAPPORT code followed by description of the data produced by RAPPORT and FERMAT and the data from the measurements. In the following sections we first compare the data qualitatively followed by a target discrimination analyse where also data from other targets (T72, T62 and BMP) are used. We finally summarise and give conclusions.

van den Broek, B.; Bieker, T.; van Ewijk, L. (2005) Comparison of Modelled to Measured High-Resolution ISAR Data. In *MMW Advanced Target Recognition and Identification Experiment* (pp. 17-1 – 17-10). Meeting Proceedings RTO-MP-SET-096, Paper 17. Neuilly-sur-Seine, France: RTO. Available from: http://www.rto.nato.int/abstracts.asp.

Report Documentation Page

Form Approved
OMB No. 0704-0188

1. REPORT DATE	2. REPORT TYPE	3. DATES COVERED
01 MAY 2005	**N/A**	**-**

4. TITLE AND SUBTITLE	5a. CONTRACT NUMBER
Comparison of Modelled to Measured High-Resolution ISAR Data	5b. GRANT NUMBER
	5c. PROGRAM ELEMENT NUMBER
6. AUTHOR(S)	5d. PROJECT NUMBER
	5e. TASK NUMBER
	5f. WORK UNIT NUMBER
7. PERFORMING ORGANIZATION NAME(S) AND ADDRESS(ES) **TNO Defense, Security and Safety, Waalsdorperweg 63, 2509 JG The Hague, The Netherlands**	8. PERFORMING ORGANIZATION REPORT NUMBER
9. SPONSORING/MONITORING AGENCY NAME(S) AND ADDRESS(ES)	10. SPONSOR/MONITOR'S ACRONYM(S)
	11. SPONSOR/MONITOR'S REPORT NUMBER(S)

12. DISTRIBUTION/AVAILABILITY STATEMENT
Approved for public release, distribution unlimited

13. SUPPLEMENTARY NOTES
See also ADM202152., The original document contains color images.

14. ABSTRACT

15. SUBJECT TERMS

16. SECURITY CLASSIFICATION OF:			17. LIMITATION OF ABSTRACT	18. NUMBER OF PAGES	19a. NAME OF RESPONSIBLE PERSON
a. REPORT	b. ABSTRACT	c. THIS PAGE			
unclassified	**unclassified**	**unclassified**	**UU**	**27**	

Standard Form 298 (Rev. 8-98)
Prescribed by ANSI Std Z39-18

2. The RAPPORT RCS prediction code

The code, “Radar signature Analysis and Prediction by Physical Optics and Ray Tracing" (RAPPORT), is developed by TNO to predict the Radar Cross Section (RCS). It is a high-frequency technique, implying that it is suitable for complex objects that are much larger than the wavelength of the radar radiation. It is used to predict the RCS of targets, such as ships, vehicles and aircrafts, to generate inverse synthetic aperture radar (ISAR) images of such targets, and to evaluate the effect of RCS reduction measures. The implemented algorithm is based upon a combination of Physical Optics (PO) and Geometrical Optics (GO), as proposed in Knott (1981). Objects have to be described as a collection of flat polygonal plates (facets), because of the adopted method to solve the PO integral (see Gordon, 1975).
RAPPORT makes use of an efficient backward ray-tracing algorithm, controlled by user-defined parameters, to construct the illuminated part of the object, from which the RCS can be computed for any desired number of reflections and frequencies. For every flat facet in the object description it is determined whether this facet is visible for the incident radiation by shooting a ray at the centre of this facet. When the centre of the facet is not blocked by another part of the object the complete facet is treated as visible.
Multiple reflections are possible up to any level. For every multiple reflection path the original incident radiation is reflected using Snells law of reflection and the thus obtained new direction of propagation is used as direction of incidence on any other part of the object. The major difference with single reflection lies in the fact that not only the facet is checked for visibility for the incident field, but also for the reflected field. This is necessary because a facet might be illuminated by multiple interactions whereas there is no direct way of the radiation towards the receiver.
Polarisation is taken into account by decomposing the incident fields at every reflection in two orthogonal components and treating both components separately. After each reflection the fields are combined again forming the scattered field by that facet. It must be noted that polarisation dependent scattering will only be present in case of multiple reflections. If the incident field is singly reflected back towards the receiver, RAPPORT will produce the same result irrespective the polarisation. This is caused by the fact that PO is used, which is inherently polarisation independent. Two linear polarisations can be used, from which all other possible polarised fields can be constructed.

3. Description of data

The object used for this research is the ZSU23-4, a USSR air defence tank, of which high resolution ISAR measurements were made available to the NATO/SET069 working group by ARL. Various facet models for the geometrical description exist. For the NATO/SET069 group a medium fidelity model consisting of approximately 60.000 triangular facets and a high fidelity model consisting of about 600,000 facets are available. We have used here the high fidelity model to generate high-resolution ISAR data, where the parameters of the ISAR data correspond exactly with those of the measured ISAR data. In figure 1 images of the tank and the 600,000 facet model are shown.

Figure 1. Picture of the ZSU-23 (left) and the high fidelity facet model (right) of the ZSU23-4 used by the calculations. The different facets are indicated by various colours in the lower-right frame.

The main common properties of both the measured as well as the modelled data are summarised in table 1.

Table 1. Common properties of data

Band	Ka
Centre frequency	34.25 GHz
Bandwidth	1500 MHz
Frequency step	5.86 MHz
Nr. of samples (range)	256
Angle sampling interval	0.015º
Depression angle	12º

The ISAR data from RAPPORT have been calculated for a complete aspect angle range of 360 degrees and for the HH and VV polarisation combinations. Calculations were performed by TNO on a single 2 Ghz PC using a Linux operating system and by FGAN-FHR on a 64 node 1.3 Ghz Linux cluster. Calculation times were about 10 and 2 minutes for each range line containing 256 frequency steps at TNO and FGAN, respectively.
Using the same facet model and parameters ISAR data have calculated using the FERMAT RCS prediction code from Onera. For a description of the FERMAT code we refer to Berges et al. (2004). The aspect angle range covered 180 degrees of aspect angle from –90 to 90 degrees, where at zero degrees of aspect the front target was illuminated. Data were calculated for the VV and HV polarisation combinations. An analysis of the FERMAT data will be given by Mametsa et al. (MATRIX, 2005). In this paper we only use the VV polarisation for comparison.
ISAR measurements for the ZSU23-4 were performed by ARL and were obtained using a fully polarimetric (HH, HV, VH and VV) stepped frequency radar for the complete aspect angle range of 360 degrees. Similar measured data for two other targets (T72 and BMP) have

been used in this paper for comparison. The only difference in measurement parameters is the depression angle, which was 10 degrees instead of 12 degrees, for these targets compared to the ZSU23-4 target.

4. Qualitative comparison of imagery

The measured and modelled data are in the frequency domain and spatial domain imagery is obtained through a 2-D inverse FFT (Chen and Andrews 1980). Hamming weighting was applied to reduce the sidelobes of the impulse response. Using the complete range of 256 frequency steps and 160 lines of aspect images are obtained with 10 cm resolution both in range and cross-range. We have calculated one image per degree of aspect angle implying a set of 360 10-cm resolution images for the complete aspect angle range from the RAPPORT ISAR data and ARL measurements. The FERMAT data obviously only permitted 180 images for 180 degrees of aspect. We only use the VV polarisation which all data-sets have in common. In figure 2 we show for one aspect angle an image for the RAPPORT code, FERMAT and the ARL measurements.

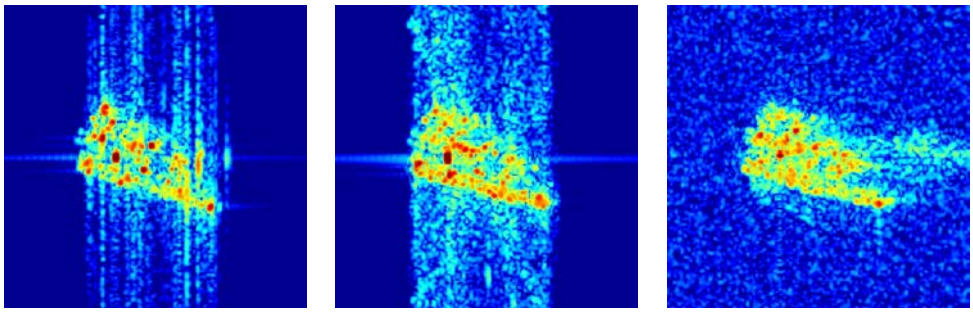

Figure 2. Simulated ISAR 10 cm resolution images for the ZSU targets. To the left RAPPORT and in the middle Fermat data are shown. Measured ISAR data from ARL are shown to the right

In figure 3 we show for comparison 10 cm ARL-ISAR images for the T72 and BMP targets for the same aspect angle compared with the image as in figure 2.

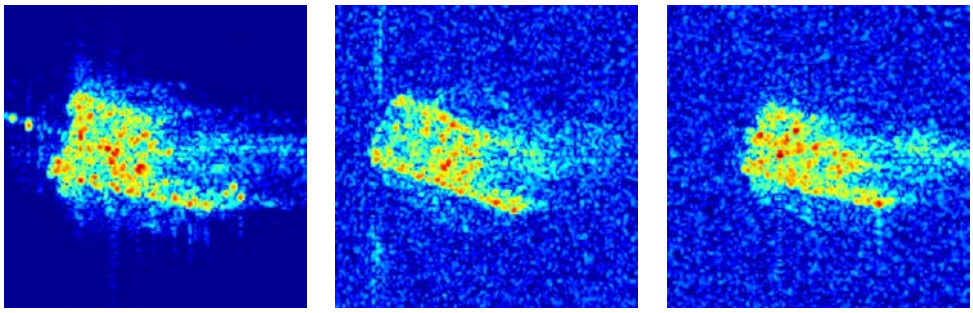

Figure 3. ARL measured ISAR 10 cm resolution images for the T72 (left) and BMP (middle) and ZSU (right) target.

When we inspect the imagery in figure 2 the general appearance of the imagery matches quite well. For example the shape is comparable for both the modelled and measured data and also the scattering from the long side of the target is present in all three images. A detailed comparison however reveals differences. The scattering of the measured data is more diffuse compared to the modelled data where point scattering is much more pronounced. This is especially true for the RAPPORT data. Also often the point scattering does not correspond between the three cases with a clear exception for the strongest point in the middle of the targets. Comparison with the targets in figure 3 shows the same kind of diffuse scattering for all three measured targets. Here it is clear that the shape is different and depends on the target type.

5. Quantitative analysis

In previous section we compared the data by visual inspection. Crucial question is whether modelled data can be used for target recognition and target discrimination. We therefore want to determine whether measured and modelled data for one target are sufficiently comparable compared to data for the other targets. For a quantitative analysis we will compare the data on basis of several features. Single features are not very suitable for target discrimination (van den Broek at al., 2003). In order to get better discrimination results we combine single features into feature vectors and consider the feature values for the different targets as multidimensional clusters in a multidimensional feature space where the dimension corresponds to the number of features used. The data from the three measured targets and the 2 modelled data-set form 5 clusters in the feature space. We analyse how well these clusters can be separated. In the ideal situation that modelled data resemble the measurements perfectly well we would expect that the clusters of modelled data and measured data of the ZSU23-4 would coincide. Using a target discrimination procedure resulting in a confusion matrix we would expect maximal confusion between the measured and modelled data and equal confusion of these data with the data from the two other comparison targets.
In the next section we will first introduce the features and show examples of the features in a 2-dimensional feature space. Next we will apply a separability measure for a multidimensional feature space and finally calculate the confusion between modelled and measured data using a maximum likelihood classifier.

5.1 Features for target discrimination

For this study we selected three radiometric and three geometric features. Table 2 summarises the features used. For a detailed description of the features we refer to van den Broek et. al. (MATRIX, 2005) No polarimetric features were considered here since only the VV polarisation was in common for the measurements, RAPPORT data, and FERMAT data.

Table 2. Overview of features used

radiometric		*geometric*	
MEAN	mean intensity	*AREA*	area of target
CVAR	coefficient of variation	*NN*	neighbour number
WFR	Weighted rank fill ratio	*LAC*	lacunarity index

As a basis to calculate the feature values, we first used a CFAR detector (Novak and Hesse, 1991) to detect target pixels. To obtain the so-called CFAR masks we used dB scaled imagery with a CFAR constant chosen at an average backscatter level of the pixels in the target area in dB scaled VV polarised images. In this way CFAR mask covers the pixels with stronger scattering from the target and almost no background pixels. Figure 4 shows examples of the CFAR masks corresponding to the images shown in figure 2.

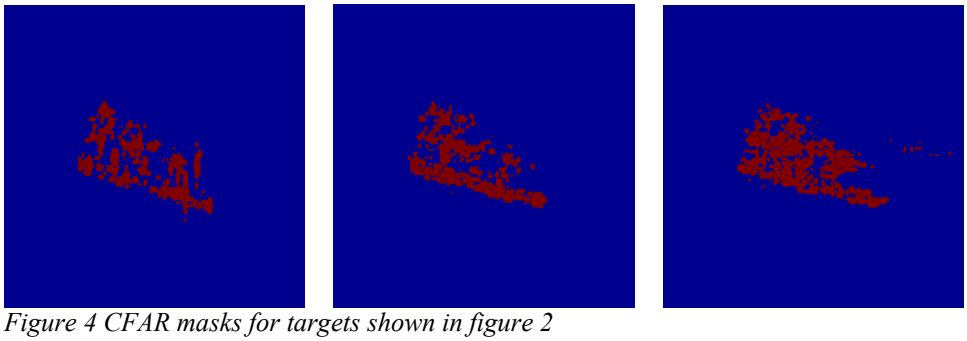

Figure 4 CFAR masks for targets shown in figure 2

As mentioned above we will analyse the features using features vectors in a multi-dimensional feature space. We show here an example of a two-dimensional case, where feature MEAN is plotted against feature AREA. This is done for the two modelled and the measured ZSU targets in figure 5 and for the three measured targets in figure 6.

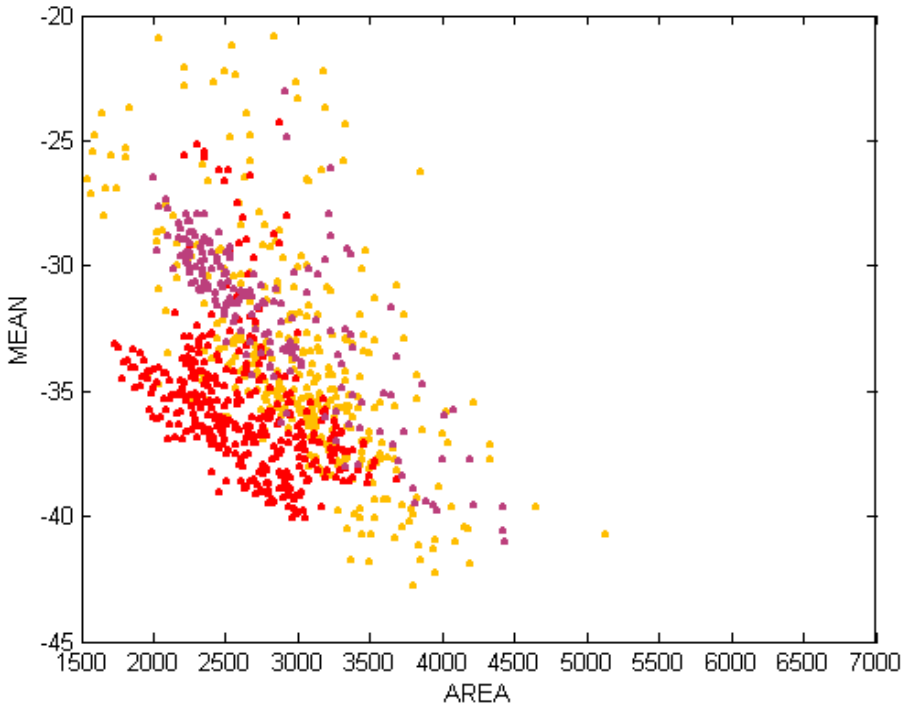

Figure 5 Feature MEAN plotted against feature AREA for the RAPPORT data (orange), the FERMAT data (purple) and for the measured ZSU data (red).

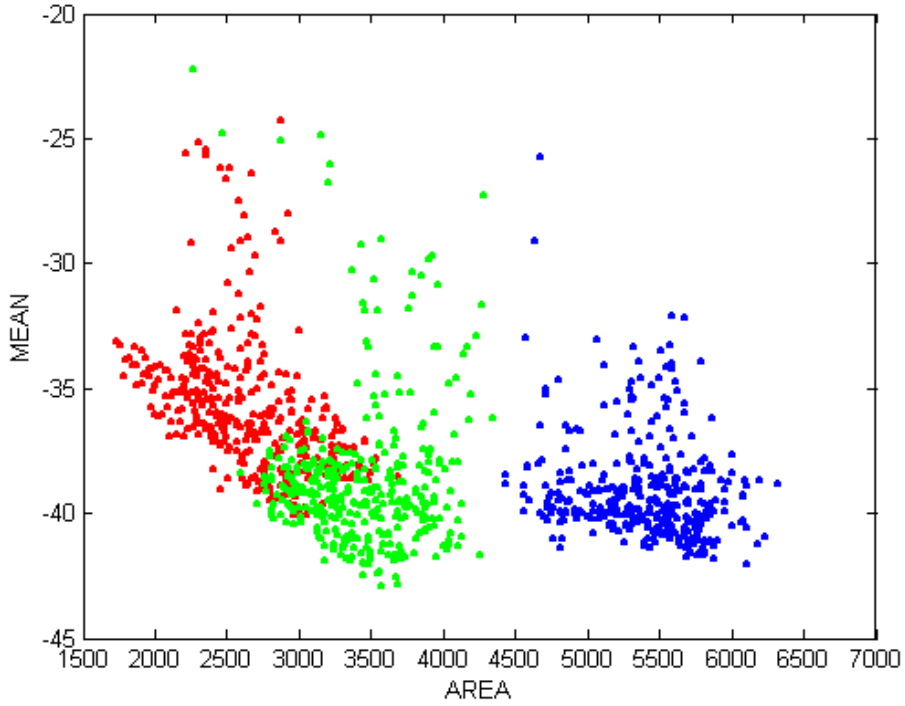

Figure 6 Feature MEAN plotted against feature AREA for the measured data. ZSU (red), T72 (blue), and BMP (green).

5.2 Separability in feature space

For the targets (measured and modelled) we have constructed 6-dimensional multi-variate target distributions where the elements of the distributions are feature vectors composed of the 6 single features mentioned in table 2 at the various aspect angles. Using means and covariance matrices derived from these clusters we have calculated a measure for the separability between the targets. The measure used here is the Bhattacharyya distance (Fukunaga, 1990). The mean feature vector and the covariance matrix are calculated for each distribution following:

$$\mu_j = \frac{1}{N}\sum_{i=1}^{N}\vec{x}_i \,, \tag{1}$$

$$\Sigma = \frac{1}{N}\sum_{i=1}^{N}(\vec{x}_i - \vec{\mu}_j)(\vec{x}_i - \vec{\mu}_j)^T \,, \tag{2}$$

where N is the number of aspect angles (360) used, i is aspect angle index, and j indicate the measured or modelled targets. The Bhattacharyya distance is then given by

$$d_{kj} = \frac{1}{8}(\vec{\mu}_k - \vec{\mu}_j)^T\left(\frac{\Sigma_k + \Sigma_j}{2}\right)^{-1}(\vec{\mu}_k - \vec{\mu}_j) + \frac{1}{2}\log\left|\frac{\Sigma_k + \Sigma_j}{2}\right| - \frac{1}{4}(\log|\Sigma_k| + \log|\Sigma_j|) \tag{3}$$

where k,j are targets indices. The Bhattacharyya distance can be considered as the multi-dimensional extension of the one dimensional separability measure:

$$d_{kj} = (\mu_k - \mu_j)^2/(\sigma_k^2 + \sigma_j^2) \tag{4}$$

where for simplicity the 'log' term has been ignored. Note that these separability measures are based on the assumption that the distributions are Gaussian (normal), which is not necessarily always the case. When the distance between two distributions is significantly larger than 1 they are in general well separable and that significant confusion is expected when the distance is smaller than 1. In table 3 we show the Bhattacharyya distances between the three measured targets BMP, T72 and ZSU and the modelled data for the ZSU, where the modelled data are indicated by RAP and FER for the RAPPORT and FERMAT respectively.

Table 3 Bhattacharyya distances

	BMP	T72	ZSU	FER	RAP
BMP	0	4.73	1.72	1.26	0.88
T72		0	8.01	4.50	4.26
ZSU			0	1.43	1.61
FER				0	0.50
RAP					0

The matrix shown by the table is symmetric since interchange of targets should not have an effect and therefore only the upper part of the table is filled for clarity.
When modelled and measured data are similar enough compared to the other targets we expect that the distances between modelled and measured ZSU data would be small compared to the distance between ZSU and the other targets.
This is certainly true for the T72 target, which shows the largest distances to all other targets. This also can be seen in figure 5 and 6 where the T72 cluster is quite separable from the other distributions. The distance between the modelled data from FERMAT and RAPPORT is small, which is expected of course.

However, the distance between the BMP and the ZSUs is comparable to the mutual distances of the several ZSUs. The distance between the BMP and the data of RAPPORT is even quite small so that considerable confusion is expected.

5.3 Classification method for target discrimination

Using above mentioned means and covariance matrices we can for each target and each aspect image calculate a discriminant function following:

$$d_j(\vec{x}_i) = (\vec{x}_i - \vec{\mu}_j)^T \Sigma_j^{-1} (\vec{x}_i - \vec{\mu}_j) + \log(|\Sigma_j|), \quad (5)$$

where *i* is the aspect angle index and *j* is the target index. The discriminant function is derived from the Bayes' decision rule, which also takes into account the a priori probability. Since this probability is the same for each target, the a priori probability has been omitted here. This is called maximum likelihood classification (Duda and Hart, 1973). Note that the discriminant function is only working well under the assumption of normal distributions. Using a feature vector for the 5 targets, we assign the target for which the discriminant function is a minimum. This procedure is repeated for every aspect angle. Next, we compute the confusion matrix indicating percentages of correctly and erroneously classifications. The result is shown in the following table.

Table 4 confusion matrix

	BMP	T72	ZSU	FER	RAP
BMP	81	0	1	0	18
T72	0	99	0	0	1
ZSU	1	0	87	6	6
FER	7	0	1	63	29
RAP	7	0	1	3	89

Ideally when the different kinds of target would be completely separable and the modelled and measured ZSUs would be perfectly similar, we would expect the following confusion matrix.

Table 5 ideal confusion matrix

	BMP	T72	ZSU	FER	RAP
BMP	100	0	0	0	0
T72	0	100	0	0	0
ZSU	0	0	33	33	33
FER	0	0	33	33	33
RAP	0	0	33	33	33

Comparison of table 4 and 5 shows, that the ideal case is certainly not true. The results in table 4 confirm the findings from the previous section. Most confusion is found between FER and RAP and almost no confusion is seen between T72 and the other targets, as should be. However there is also some confusion between BMP and RAP and relatively little confusion between the modelled and measured ZSU indicating that measured and modelled data are not very similar compared to measured data from other targets.

6. Summary and conclusions

We have compared high-resolution (10 cm) modelled ISAR data based on a high-fidelity facet model with corresponding measured ISAR data for the ZSU23-4 target. For comparison also comparable measured data from two other kind of targets, a T72 and a BMP were used. In the ideal case the modelled and measured data would be similar and would be distinguishable from the two other targets.

Visual inspection shows that images derived from the measured and modelled ZSU ISAR data have overall common characteristics, such as shape. The measured data have common characteristics such as a more diffuse appearance contrary to the more point-like appearance for the modelled data. This could be explained by the fact that also surface roughness plays an important role, giving rise to more diffuse scattering. Surface roughness is not yet accounted for in a model like RAPPORT.
A quantitative analysis on basis of features shows that the ideal case is not yet reached. Modelled data and measured data from the ZSU are quite separable while at the same time confusion exists between modelled data and measured data from the BMP.

References

1. Berges, A., Latger, J., Mametsa, H.J., Demr, FERMAT, a new radar simulation approach, *Onera TP 2004-219(1), S2-T25412*
2. Broek, van den, A.C., Dekker, R.J., Steeghs, T.P.H., Robustness of Features for Automatic Target Discriminaton in High Resolution Polarimetric SAR Data, *Algorithms for Synthetic Aperture Radar Imagery X, Proc. of SPIE, Vol. 5095, 2003*, pp. 242-253.
3. Broek, van den, A.C., Dekker, R.J., Target discrimination in polarimetric ISAR data using robust feature vectors, *MATRIX 2005 NATO/SET096 specialist meeting , Oberammergau, Germany.*
4. Chen, C.C., and Andrews, H.C., "Multifrequency Imaging of Radar Turntable Data", *IEEE Trans. on Aerosp. Electron. Syst., Vol. 16, No. 1*, pp. 15-22, 1980.
5. Duda, R.O., Hart, P.E., *Pattern Classification and Scene Analysis*, John Wiley and Sons, New York, 1973.
6. Fukunaga, K,. 1990, *Introduction to Statistical Patten Recognition*, Academic Press Inc., Boston.
7. Gordon, W.B., 1975, 'Far field approximation to the Kirchoff-Hclmholtz representations of scattered fields'*, IEEE Transactions on Antennas and Propagation*, Vol.23, pp.590-592
8. Knott, E.F. , 1981, 'A tool for predicting the Radar Cross Section of an arbitrary trihedral corner', *IEEE South East Conference*, pp. 17-20
9. Mametsa, H.J., Berges, A., Taking into account surface roughness, impact on ISAR images calculating the ZSU23-4*, MATRIX 2005 NATO/SET096 specialist meeting , Oberammergau, Germany.*
10. Novak, L.M., S.R. Hesse, S.R., "On the performance of order-statistics CFAR detectors", *IEEE Conference Record of the 25th Asilomar Conference on Signals, Systems and Computers, Vol.2*, pp. 835-840, 1991.

Comparison of modelled and measured high-resolution ISAR data

TNO Defense, Security & Safety

TNO | Knowledge for business

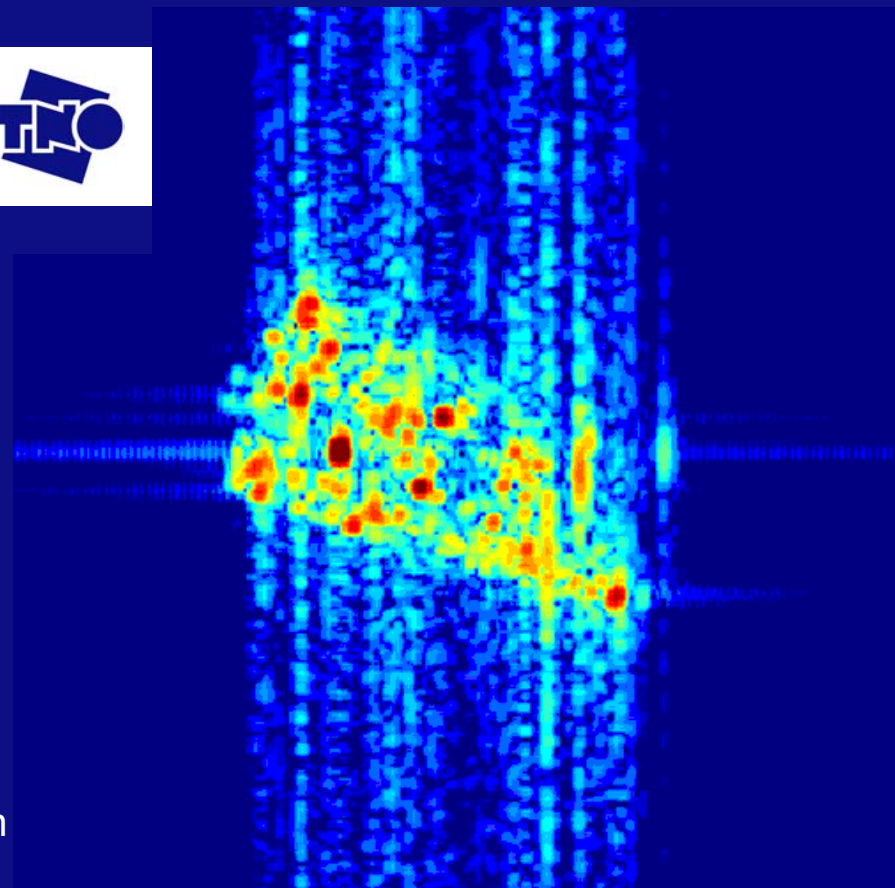

Bert van den Broek, Tanja Bieker, Lucas van Ewijk

Matrix Specialist Meeting
10-12 May 2005 Oberammergau

Outline

- Modelling & measurements
- RAPPORT code
- Facet models
- Images
- Analysis with features
- Summary

Modelling versus measurements

- Measurements are time consuming and expensive
- Modelling is more flexible
- High fidelity facets models become available
- Computing power increases so that practical application becomes feasible
- But … can modelling replace measurements, i.e. are modelled and measured data similar enough for target discrimination.

Modeling - it all starts with the radar equation

$$P_r = \frac{G_t P_t}{4\pi R^2} \frac{\sigma}{4\pi R^2} A_{eff}$$

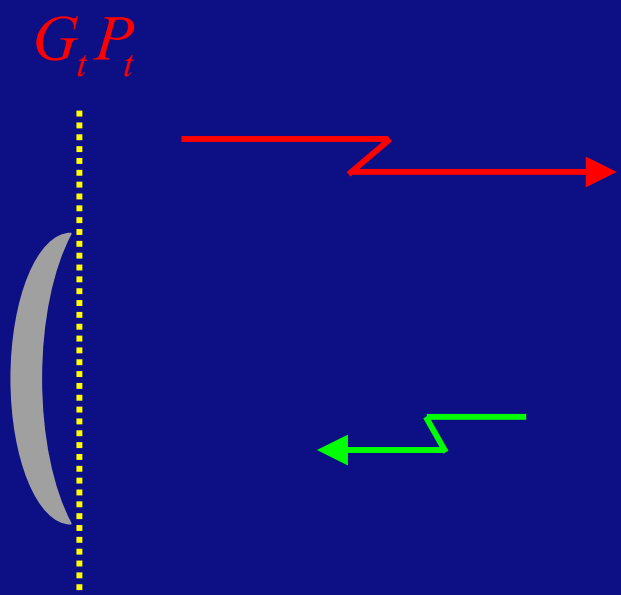

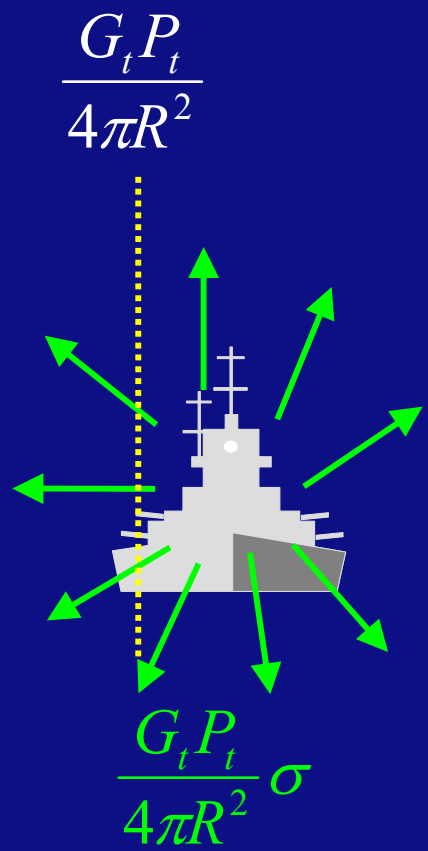

Scattering mechanisms

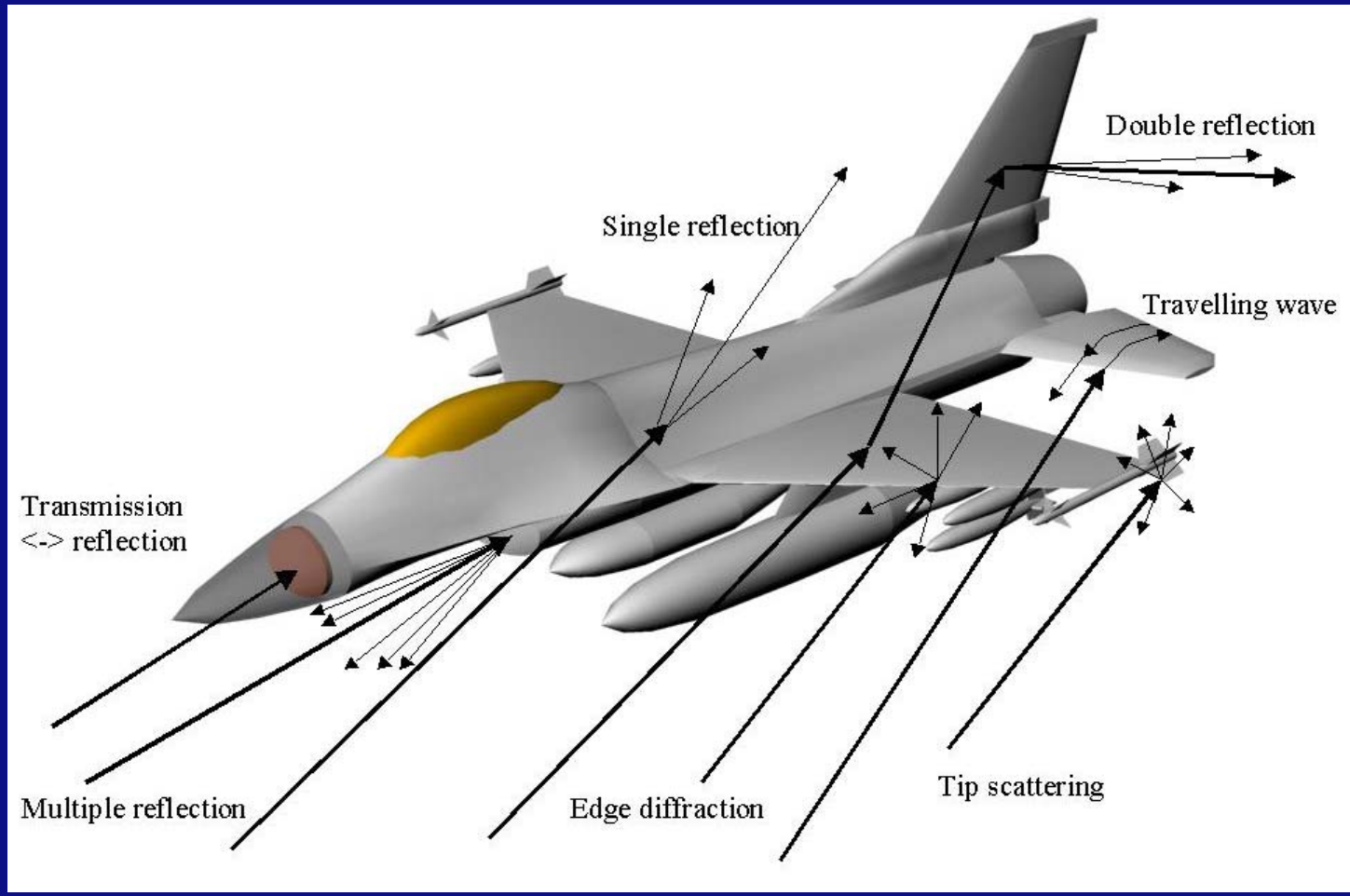

Radar signature Analysis and Prediciton by Physical Optics and Ray Tracing (RAPPORT)

RCS prediction of complex objects by combining Physical Optics (PO) and ray tracing.

- Facetised object description
- Fully polarimetric
- Multiple reflections using a frequency independent ray tracing scheme
- Ray tracing using domain decomposition techniques
- Computation of complex data in far-field and near-field
- Monostatic and bistatic
- Antenna pattern included
- Multipath possible using a “pattern propagation factor” formalism

RAPPORT features

Shadowing

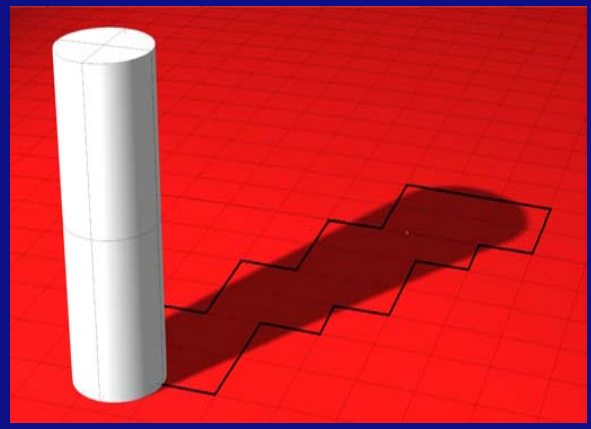

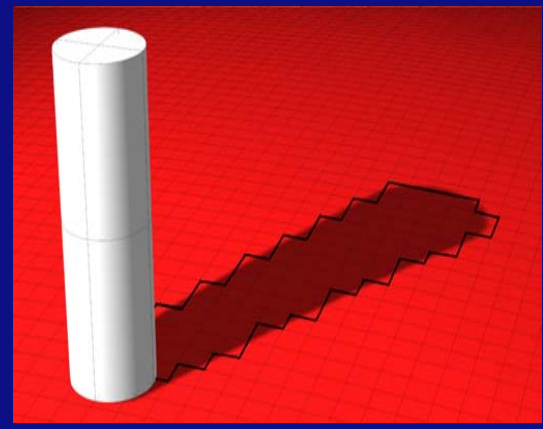

No surface roughness

No diffraction taken into account in this study

Facet models of ZSU23-4

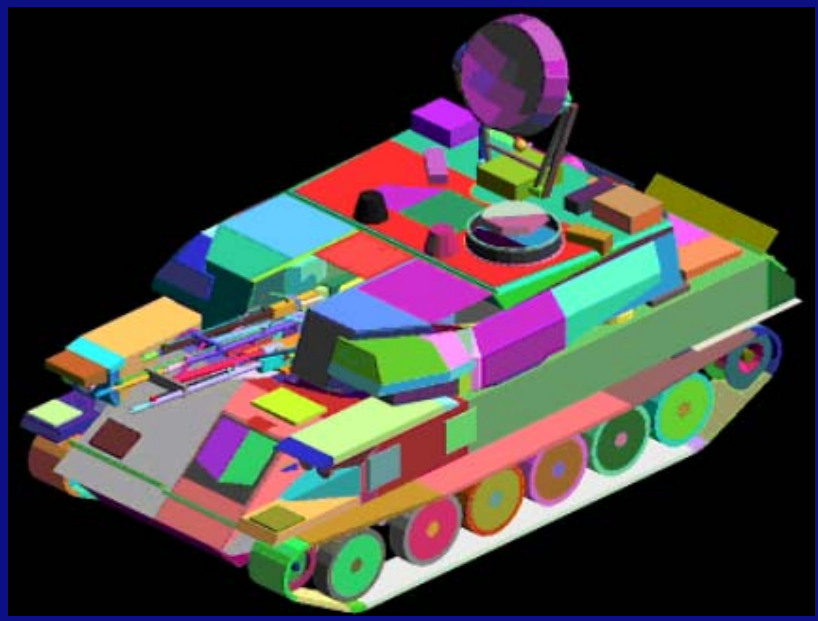

60,000 facets

600,000 facets

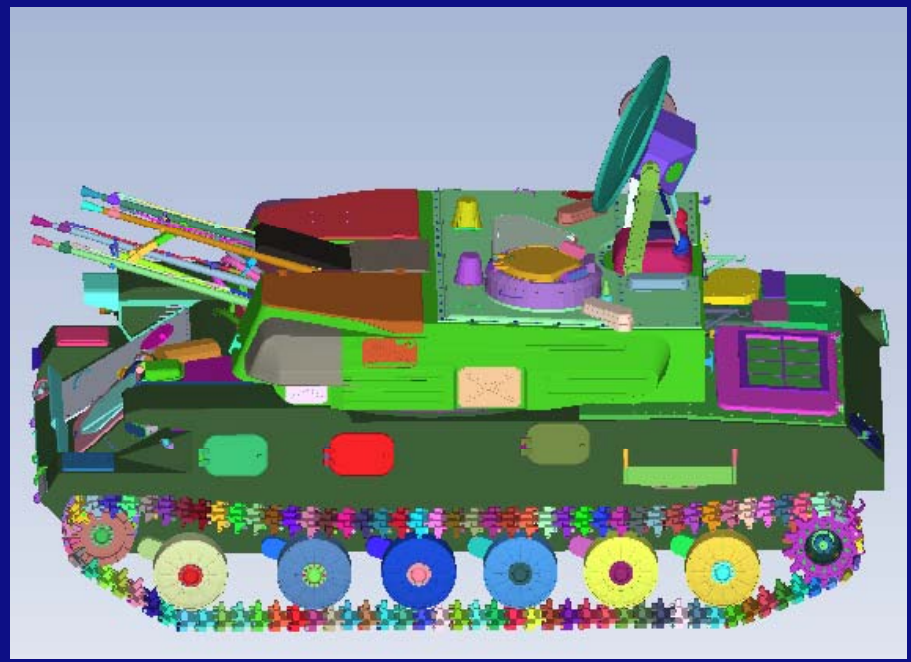

Images from RAPPORT

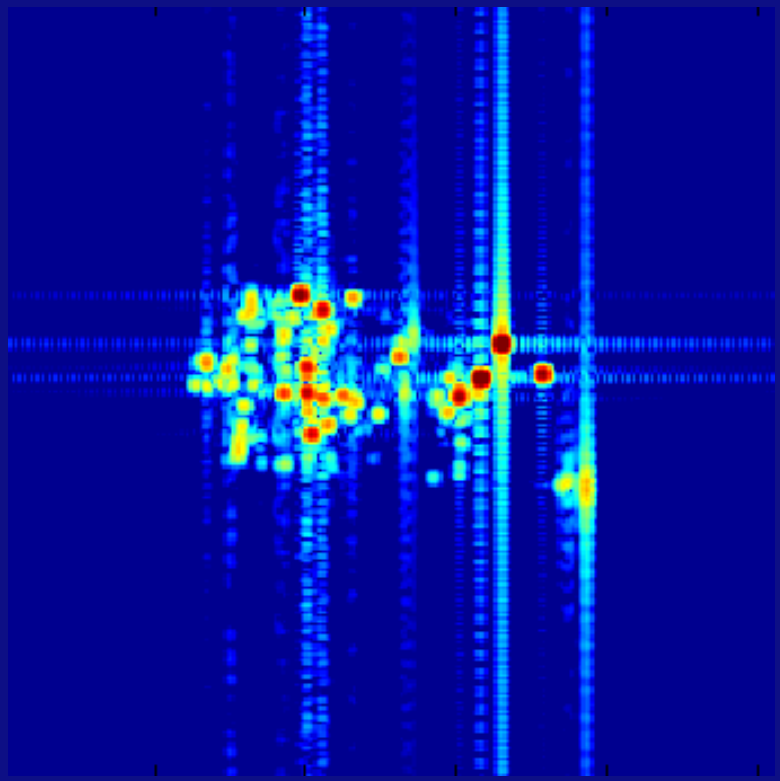

60,000 facets

600,000 facets

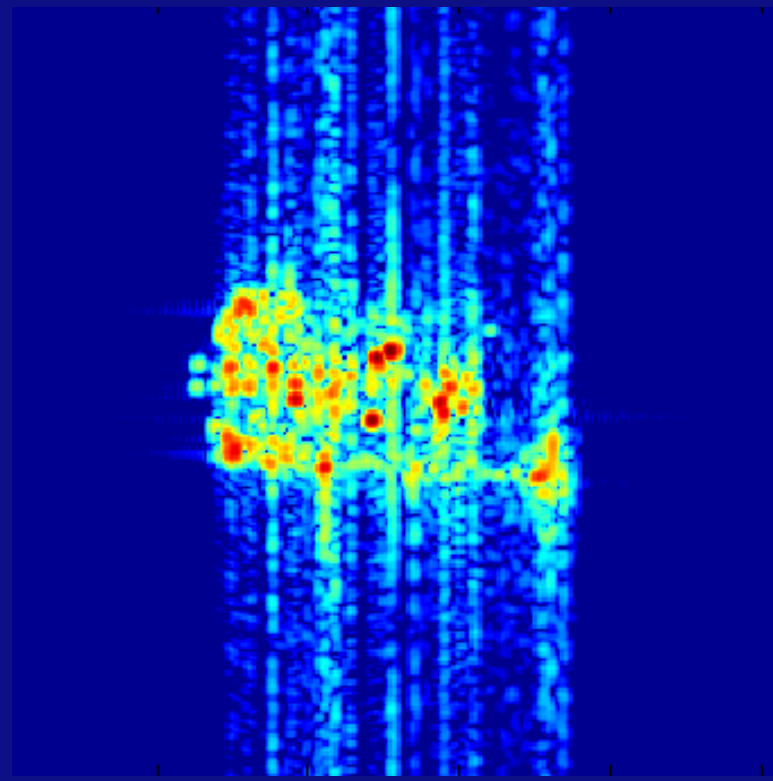

Calculation time:
2-10 minutes for 256 frequencies

Comparison images from modelling with measurements

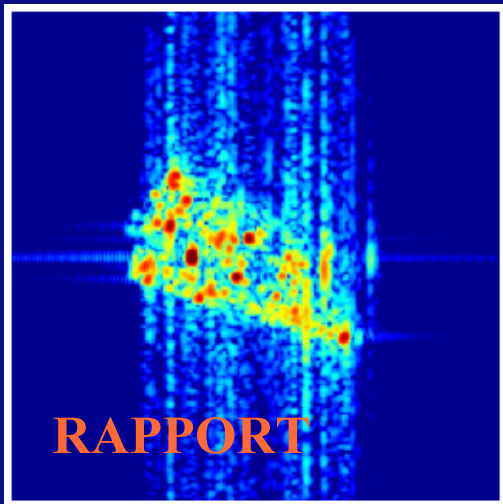

10 cm resolution

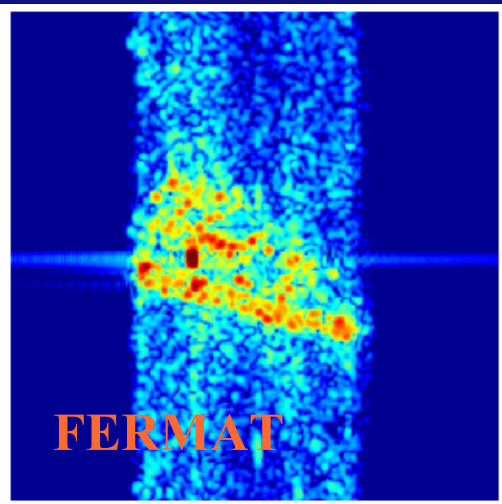

FERMAT RCS code
Onera - Toulouse

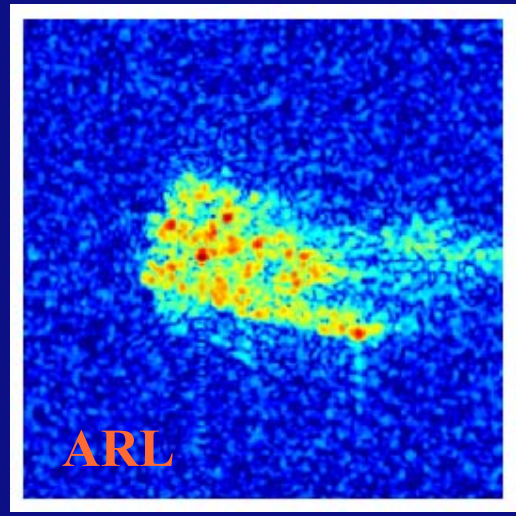

Measurements by
Army Research Laboratory
(ARL)

Band	Ka
Centre frequency	34.25 GHz
Bandwidth	1500 MHz
Frequency step	5.86 MHz
Nr. of samples (range)	256
Angle sampling interval	0.015°
Depression angle	12°

Other measurements for comparison

Same observation parameters as for modelling
except depression angle 10 degrees for BMP and T72

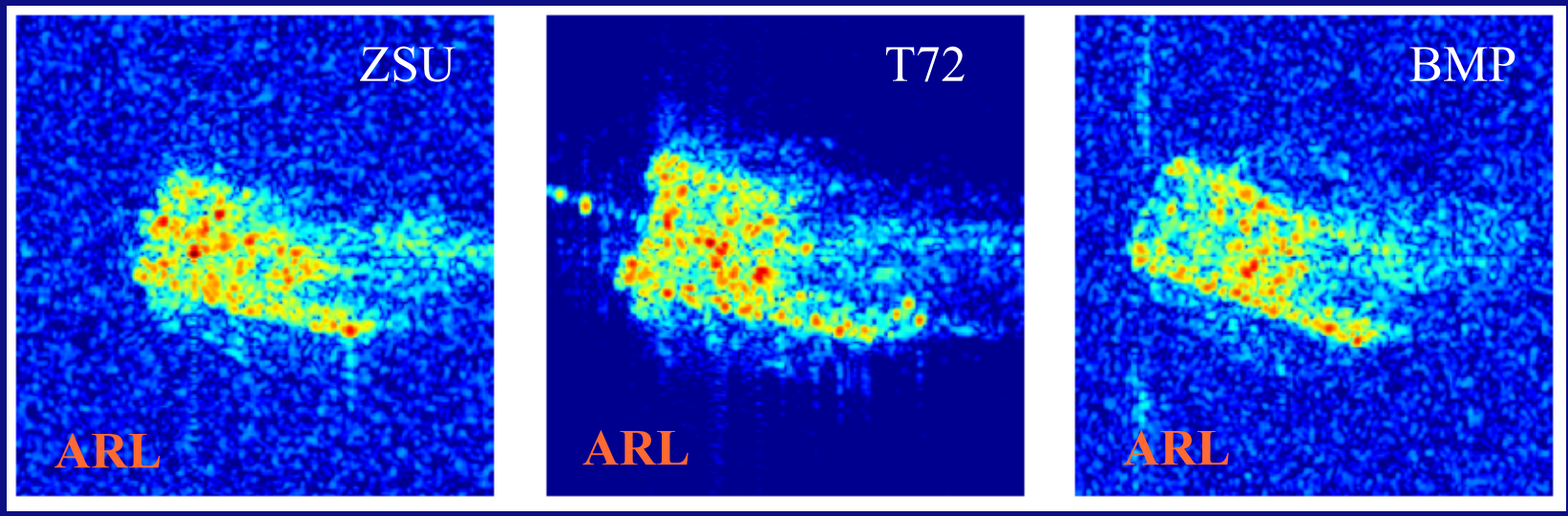

Features used for comparison

radiometric		*geometric*	
MEAN	mean intensity	*AREA*	area of target
CVAR	coefficient of variation	*NN*	neighbour number
WFR	Weighted rank fill ratio	*LAC*	lacunarity index

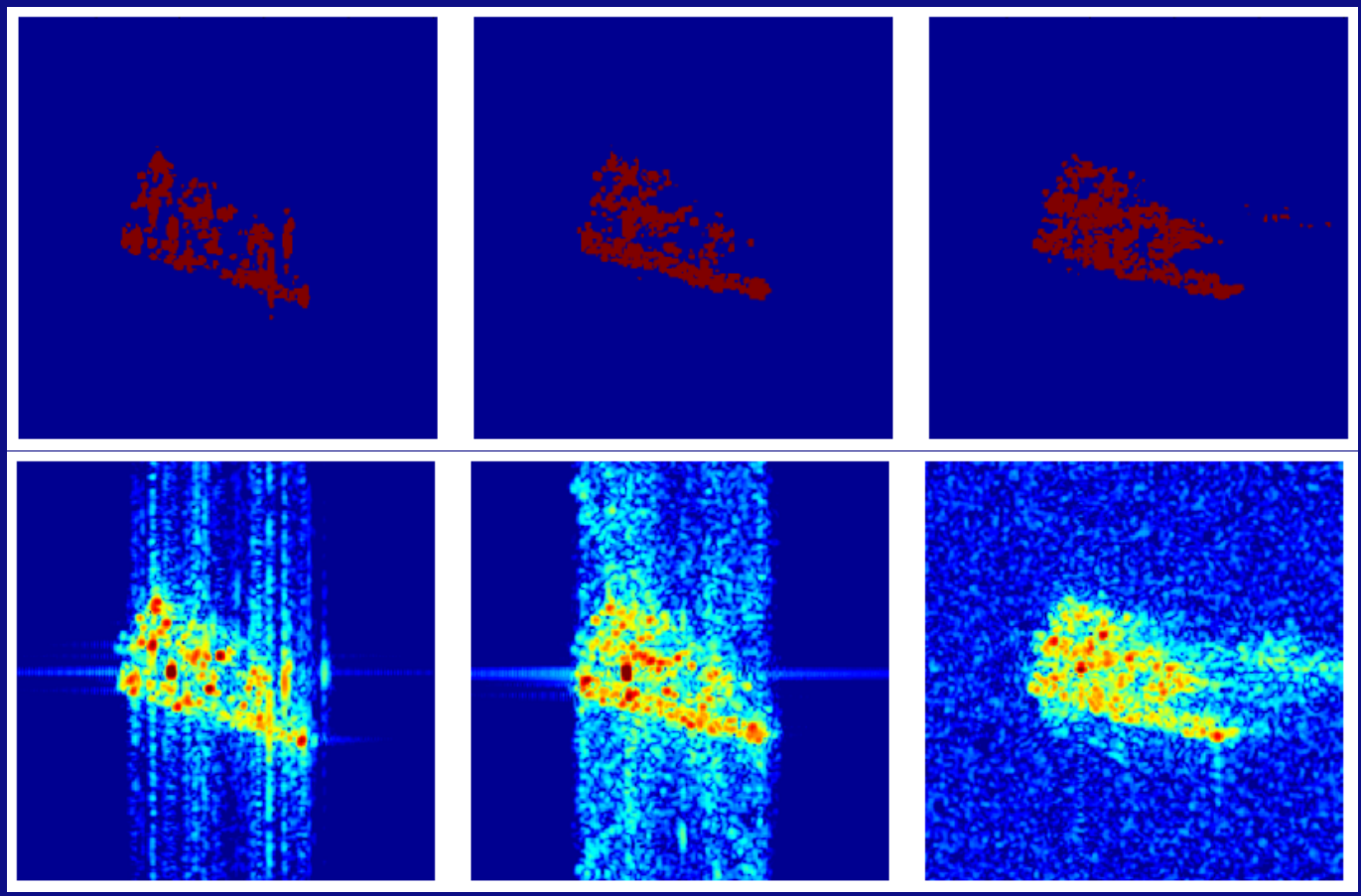

CFAR masks (ZSU)

Only VV Polarisation used

Examples of feature scatter plots

Red: ZSU-ARL
Green: BMP-ATL
Blue: T72-ARL

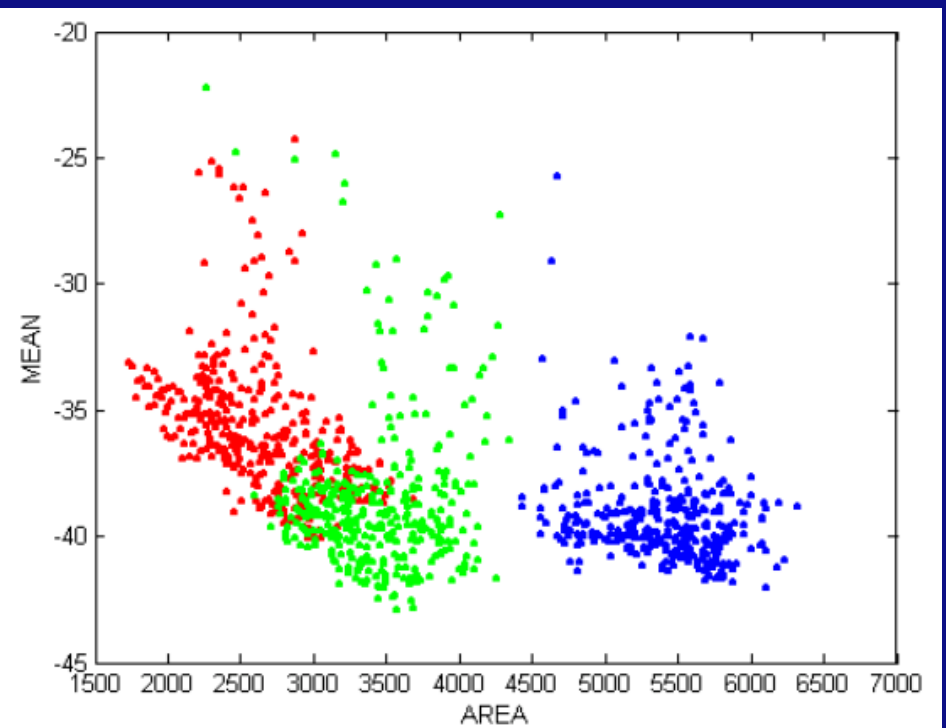

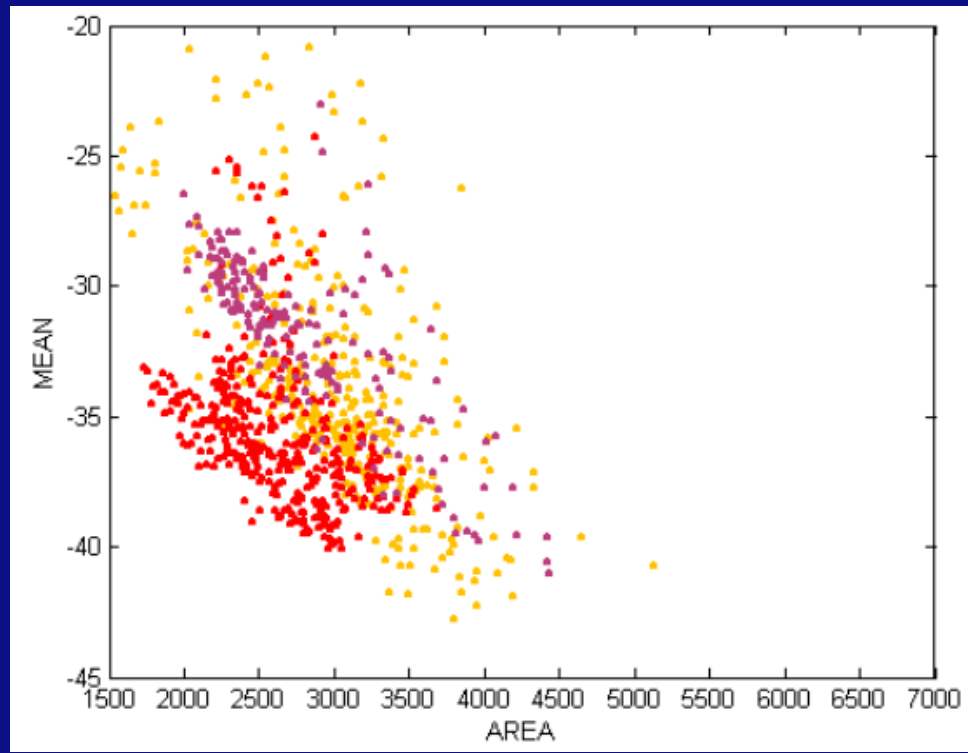

Red: ZSU-ARL
Orange: RAPPORT
Purple: FERMAT

Separability in feature space

Cluster statistics

Feature vector $\vec{x} = [MEAN, CVAR, WFR, AREA, NN, LAC]^T$

Mean $\mu_j = \frac{1}{N}\sum_{i=1}^{N}\vec{x}_i$

Covariance matrix $\Sigma = \frac{1}{N}\sum_{i=1}^{N}(\vec{x}_i - \vec{\mu}_j)(\vec{x}_i - \vec{\mu}_j)^T$

Bhattacharyya distance $d_{kj} = \frac{1}{8}(\vec{\mu}_k - \vec{\mu}_j)^T\left(\frac{\Sigma_k + \Sigma_j}{2}\right)^{-1}(\vec{\mu}_k - \vec{\mu}_j) + \frac{1}{2}\log\left|\frac{\Sigma_k + \Sigma_j}{2}\right| - \frac{1}{4}(\log|\Sigma_k| + \log|\Sigma_j|)$

i aspect angle index k,j target index

Distance between clusters

Bhattacharyya distance

	BMP	T72	ZSU	FER	RAP
BMP	0	4.73	1.72	1.26	0.88
T72		0	8.01	4.50	4.26
ZSU			0	1.43	1.61
FER				0	0.50
RAP					0

Bhattacharyya distance

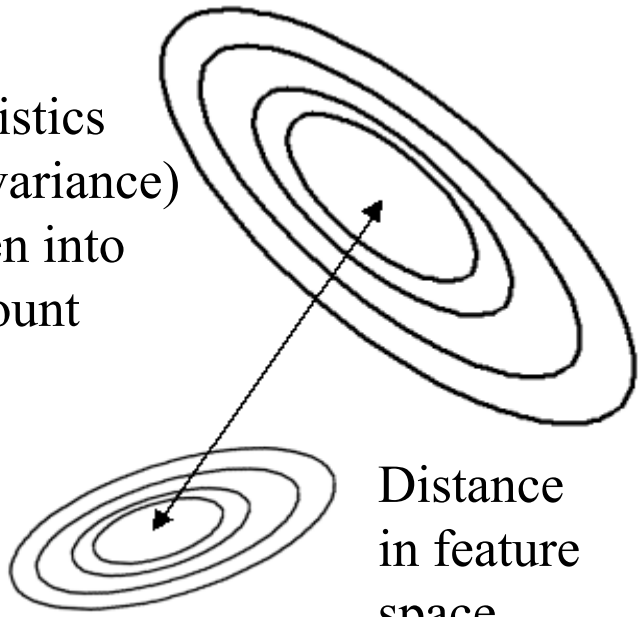

T72 shows largest distances

Small distance between FER and RAP (expected)

ZSU measured & modelled have intermediate distances

BMP and RAP have a small distance

Target discrimination

$$\mu_j = \frac{1}{N}\sum_{i=1}^{N}\vec{x}_{ij}$$

$$\Sigma_j = \frac{1}{N}\sum_{i=1}^{N}(\vec{x}_{ij} - \vec{\mu}_j)(\vec{x}_{ij} - \vec{\mu}_j)^T$$

$$d_j(\vec{x}_i) = (\vec{x}_i - \vec{\mu}_j)^T \Sigma_j^{-1}(\vec{x}_i - \vec{\mu}_j) + \log(|\Sigma_j|)$$

N = number of aspect angles used

Target $j \in$ {T72, T62, BMP, ZSU}

x_l = feature vector for aspect angle l

d_j = discriminant function

	BMP	T72	ZSU	FER	RAP
BMP	81	0	1	0	18
T72	0	99	0	0	1
ZSU	1	0	87	6	6
FER	7	0	1	63	29
RAP	7	0	1	3	89

Confusion matrix

	BMP	T72	ZSU	FER	RAP
BMP	100	0	0	0	0
T72	0	100	0	0	0
ZSU	0	0	33	33	33
FER	0	0	33	33	33
RAP	0	0	33	33	33

Reference confusion matrix

- Confusion between BMP and RAP
- Measured ZSU is quite separable from modelled ZSU

Summary

- Modelled & measured data look similar, but are different in detail
- Measured images are more diffuse
- Modelled images show more point-like scattering
- Due to influence of surface roughness ?
- Modelled and measured data for ZSU are separable
- Confusion exists between measured BMP and modelled ZSU
- Modelled data is not yet good enough to replace measurements for target discrimination